Biochemistry and Biophysics Reports 32 (2022) 101333

Contents lists available at ScienceDirect

Biochemistry and Biophysics Reports

journal homepage: www.elsevier.com/locate/bbrep

Effects of zinc and carnosine on aggregation kinetics of Amyloid-β40 peptide

Fengyun Shen, Deepika Regmi, Majedul Islam, Dawn Raja Somu, Vivian Merk, Deguo Du *

Department of Chemistry and Biochemistry, Florida Atlantic University, Boca Raton, FL, 33431, USA

A B S T R A C T

The accumulation and amyloid formation of amyloid-β (Aβ) peptides is closely associated with the pathology of Alzheimer's disease. The physiological environment wherein Aβ aggregation happens is crowded with a large variety of metal ions including Zn^{2+}. In this study, we investigated the role of Zn^{2+} in regulating the aggregation kinetics of Aβ40 peptide. Our results show that Zn^{2+} can shift a typical single sigmoidal aggregation kinetics of Aβ40 to a biphasic aggregation process. Zn^{2+} aids in initiating the rapid self-assembly of monomers to form oligomeric intermediates, which further grow into amyloid fibrils in the first aggregation phase. The presence of Zn^{2+} also retards the appearance of the second aggregation phase in a concentration dependent manner. In addition, our results show that a natural dipeptide, carnosine, can greatly alleviate the effect of Zn^{2+} on Aβ aggregation kinetics, most likely by coordinating with the metal ion to form chelates. These results suggest a potential in vivo protective effect of carnosine against the cytotoxicity of Aβ by suppressing Zn^{2+}-induced rapid formation of Aβ oligomers.

1. Introduction

Alzheimer's disease (AD) is the most common neurodegenerative disorder, and is responsible for 60–80% of all cases of dementia. One of the main hallmarks of AD is the accumulation of amyloid-β (Aβ) peptides and the formation of extracellular amyloid plaques in the brain. Aggregation and amyloid fibril formation of Aβ has been suggested to be closely associated with the pathology of AD [1], although the fundamental mechanism by which the assembly process of Aβ causes the toxicity leading to cell death still remains unclear.

The physiological environment wherein Aβ aggregation happens is crowded with a large variety of metal ions such as Zn^{2+}. Zn^{2+} is enriched in the hippocampus and neocortical region of mammalian brain [2]. The total concentration in the brain is estimated to be approximately 150 μM [3,4]. In addition, Zn^{2+} appears to co-aggregate with Aβ peptides and is enriched in senile plaques from brain tissues of AD patients [5,6]. Zn^{2+} is able to bind to Aβ by interacting with the residues at the N-terminal region [7,8], and in consequence is actively involved in the generation of Aβ amyloid fibrils and regulation of cytotoxicity of Aβ [9]. However, the mechanistic role of Zn^{2+} in modulating Aβ aggregation pathway and aggregation kinetics still remains elusive. Contradictory results of the effects of Zn^{2+} on the amyloidogenesis of Aβ have been reported in the literature. For instance, Yoshiike et al. reported that Zn^{2+} inhibits the aggregation of both Aβ40 and Aβ42 in an in vitro study [9]. Similarly, Abelein et al. also reported that the substoichiometric amount of Zn^{2+} effectively retards the generation of amyloid fibrils of Aβ under near-physiological conditions [10]. On the other hand, some other studies found that Zn^{2+} is capable of accelerating aggregation of Aβ under conditions with physiological pH in vitro [11,12]. In addition, Zn^{2+} is suggested to promote the formation of toxic and off-pathway oligomers of Aβ with reduced β-sheet content [13], or favor the formation of amorphous aggregates [14,15]. These pioneering studies clearly show a critical role of Zn^{2+} in modulating Aβ aggregation, and indicate the sensitivity of the regulatory function of this metal ion on the specific environment. The detailed kinetic effects of Zn^{2+} on Aβ self-assembly still remains to be further elucidated. In the present work, we systematically studied the impact of Zn^{2+} on the aggregation kinetics of Aβ40 using a combination of spectroscopic and imaging methods. The results suggest that the presence of Zn^{2+} converts the typical sigmoid kinetics of Aβ40 aggregation to a biphasic kinetic process, and facilitates an early aggregation kinetic phase while retarding a second aggregation phase during the aggregation of Aβ40 in phosphate buffer solution.

In addition, carnosine (β-alanyl-L-histidine), a natural dipeptide, is widely distributed in mammalian muscle and nervous tissues with high concentrations [16]. Carnosine exerts a variety of biological functions such as pH buffer modulator, antioxidant, hydroxyl radical scavenger, antiglycating agent, and chelator of metal ions such as Zn^{2+} and Cu^{2+} [17,18]. Growing amount of evidence suggests that carnosine is a neuroprotective molecule against various neurodegenerative diseases including AD [19,20]. Recent studies have also shown that carnosine inhibits Aβ aggregation in vitro and ameliorates Aβ-induced cytotoxicity [21,22]. Being a metal ion chelator, the potential modulating role of

* Corresponding author.
E-mail address: ddu@fau.edu (D. Du).

https://doi.org/10.1016/j.bbrep.2022.101333
Received 31 May 2022; Received in revised form 15 July 2022; Accepted 21 August 2022

carnosine on Zn^{2+}-mediated Aβ aggregation, however, has been little addressed. In this work, we also investigated the effect of carnosine on Aβ aggregation in the presence of Zn^{2+} to gain insight into the roles of carnosine in regulating Aβ aggregation in a metal ion-rich physiological environment.

2. Materials and methods

2.1. Synthesis and purification of Aβ40

Aβ40 was synthesized on a PS3 solid-phase peptide synthesizer (Protein Technologies Inc., Woburn, MA) using Fmoc chemistry. The crude peptide was purified by high-performance liquid chromatography (HPLC) using a C18 reverse-phase column. After purification, the

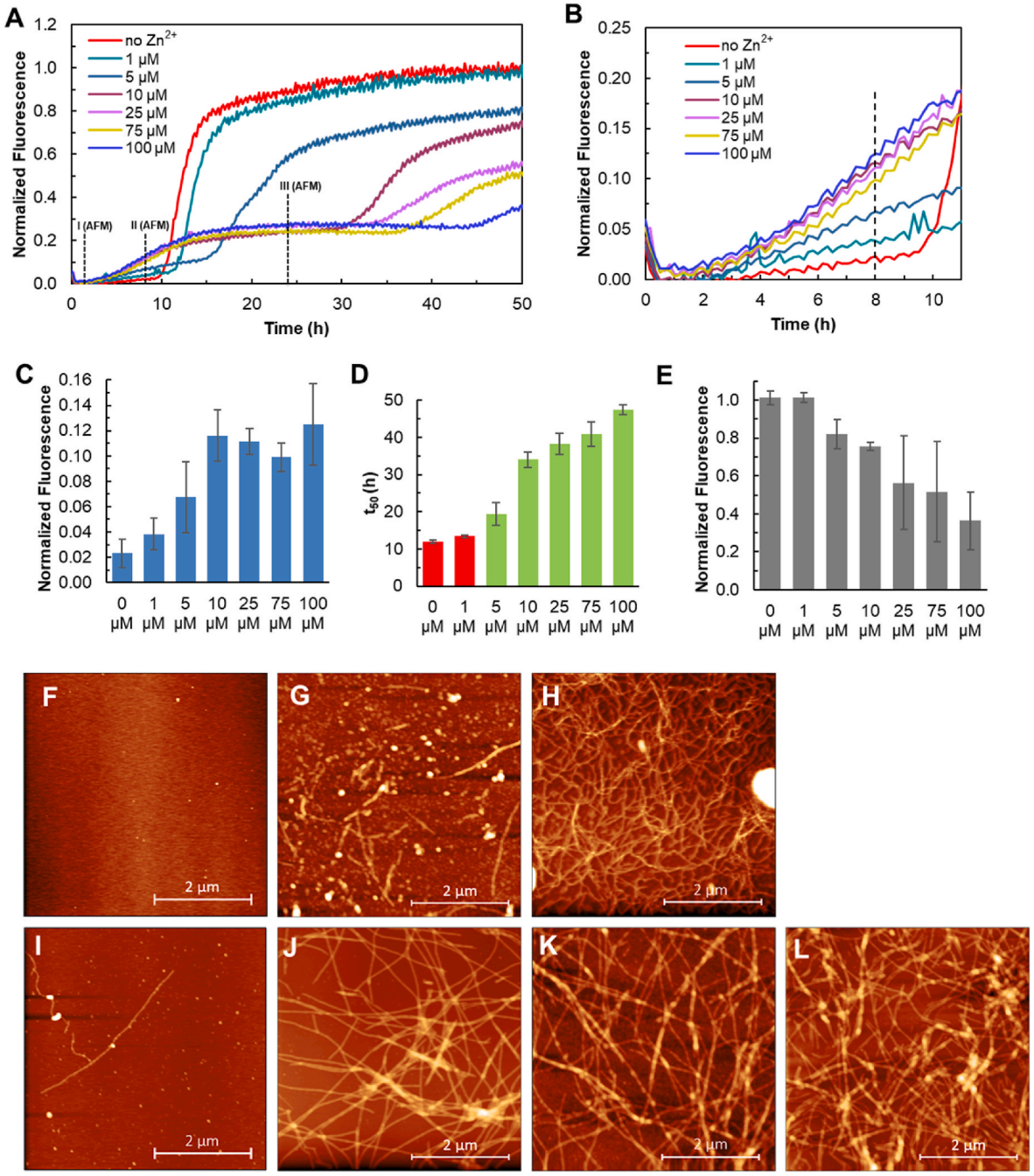

Fig. 1. Effect of Zn^{2+} on Aβ40 aggregation. (A) Aggregation kinetics of Aβ40 (10 μM) alone and in the presence of different concentrations of Zn^{2+} followed by ThT fluorescence at 37 °C in pH 7.4 phosphate buffer (50 mM Na-phosphate). (B) Expansion of the early stage of the aggregation kinetics curves shown in panel A. (C) Relative ThT fluorescence intensity at 8 h (the time point indicated in panel B) of the aggregation kinetics of Aβ40 in the absence or presence of different concentrations of Zn^{2+}. The data are reported as mean ± standard deviation of triplicate results. (D) The half time (t_{50}) of the aggregation kinetics. For aggregation of Aβ40 with Zn^{2+} of 5–100 μM, the t_{50} value of the second aggregation phase is reported. (E) Relative ThT fluorescence intensity obtained at the end of the aggregation kinetics of Aβ40 shown in panel A. (F–H) Tapping mode AFM images of Aβ40 only samples measured at the time point I indicated in panel A (F), time point II (G), and at the end of the aggregation kinetics experiment (H). (I–L) Tapping mode AFM images of Aβ40 incubated with 10 μM Zn^{2+} measured at the time point I (I), time point II (J), time point III (K), and after 3 d of incubation (L).

peptide was lyophilized to obtain powder samples. The molecular weight of Aβ40 was verified to be 4330 by matrix-assisted laser desorption ionization (MALDI) mass spectrometry. The Aβ40 peptide utilized in the study was further monomerized as described previously [23].

2.2. Kinetic aggregation assay of Aβ40 using thioflavin T (ThT)

The aggregation kinetics followed by ThT fluorescence were measured as described previously [24]. Briefly, monomerized Aβ40 peptide solution was diluted to a final concentration of 10 μM in a pH 7.4 phosphate buffer solution (50 mM Na-phosphate) which also contained 20 μM ThT. 100 μL solution was then transferred into a well of a 96-well microplate (Costar black, clear bottom). The plate was loaded into a Gemini SpectraMax EM fluorescence plate reader (Molecular Devices, Sunnyvale, CA) and incubated at 37 °C. The fluorescence (excitation at 440 nm, emission at 485 nm) was measured from the bottom of the plate at 10 min intervals, with 5 s of agitation before each reading.

2.3. Atomic force microscopy (AFM)

An aliquot of the peptide solution (20 μL) was adsorbed onto the surface of fresh mica (8 × 8 mm) for 5 min. The liquid was wicked off by absorption into filter paper. Salt and unbound materials were washed in triplicate by 20 μL of Milli-Q H_2O and removed by filter paper absorption. The samples were dried over night before measurement. The AFM images were acquired in tapping mode at a drive frequency of approximately 150 kHz using AFMWorkshop HR (Hilton Head Island, SC) with AFMWorkshop ACLA-10-W cantilevers. Multiple AFM imaging scans were performed at different spots on mica surface to ensure that the imaging results represent the morphological properties of the sample and avoid experimental bias caused by potentially inhomogeneous distribution of sample on the mica surface.

2.4. Circular dichroism (CD)

The fresh peptide sample was diluted to a final concentration of 50 μM in 10 mM phosphate buffer of pH 7.4 with a total volume of 300 μL in 1 mm path length quartz sample cuvettes. The cuvettes were incubated quiescently at 37 °C in an incubator (VWRTM). At desired time points, CD spectra were collected on a J-810 spectropolarimeter (JASCO). Five scans were averaged for each sample.

3. Results & discussion

3.1. Effect of Zn^{2+} on the kinetics of Aβ40 aggregation

The effect of Zn^{2+} on aggregation kinetics of Aβ40 was monitored by using the fluorescence of ThT. The fluorescent dye ThT interacts with β-sheet-rich structures in amyloid fibrils leading to an increase in the fluorescence intensity in the vicinity of 480 nm. As shown in Fig. 1A, the aggregation kinetics of 10 μM Aβ40 peptide in pH 7.4 phosphate buffer exhibits a typical single sigmoidal appearance containing a lag phase which is suggested to be associated with nucleation of Aβ, a fast growth phase linked to fibril elongation, and a final stationary phase indicating the formation of mature amyloid fibrils. The half time (t_{50}) of the growth phase of the Aβ40 amyloidogenesis under the current condition was approximately 12 h, where t_{50} is defined as the time at which the fluorescence intensity reaches the midpoint between the pre- and post-aggregation baselines. The addition of 1 μM Zn^{2+} slightly delays the growth phase (Fig. 1A), and the t_{50} value of the aggregation kinetics was postponed to ~13.4 h. A weak but noticeable fast increase of the ThT fluorescence intensity is observed in the lag phase of the aggregation (Fig. 1A and B). In the presence of 5 μM Zn^{2+}, the early initiation of the aggregation process becomes more significant, and the aggregation growth phase is further retarded to the t_{50} of ~19 h (Fig. 1A and B). The addition of higher concentration of Zn^{2+} leads to a more striking early aggregation phase in the kinetics (Fig. 1B), and the relative ThT fluorescence intensity during the growth of this early aggregation kinetics increases with increasing Zn^{2+} concentration (Fig. 1B and C). The appearance of this early aggregation phase observed in the presence of Zn^{2+} suggests that Zn^{2+} likely initiates a fast self-assembly of monomers and facilitates the oligomeric nucleus formation during the aggregation of Aβ, consistent with some previous reports [11–13].

The morphology of Aβ40 aggregates formed in the absence and presence of Zn^{2+} was studied by AFM imaging. As shown in Fig. 1F, at the time point I (indicated in Fig. 1A) in the early lag phase of Aβ aggregation with negligible ThT fluorescence intensity, only very few spherical oligomeric species were observed, and no fibrillar structures formed in the Aβ40 only sample. In contrast, a considerable amount of spherical oligomers was observed and a few fibrillar structures were also identified at the same time point in the Aβ40 sample with 10 μM Zn^{2+} (Fig. 1I). This is consistent with the ThT kinetics results showing that the addition of Zn^{2+} triggers a faster nucleation and aggregation of the peptide. At the time point II (Fig. 1A) of the first growth phase of the aggregation kinetics of Aβ40 with Zn^{2+}, an appreciable amount of amyloid fibrils was identified (Fig. 1J), whereas only spherical oligomers, prefibrillar and short fibrillar structures formed in the Aβ40 sample without Zn^{2+} (Fig. 1G). Taken together, both the fluorescence kinetics and the AFM imaging results indicate the role of Zn^{2+} in promoting the oligomer and fibril formation during the aggregation of Aβ.

Intriguingly, the results of the kinetics from this study show that the addition of increasing concentration of Zn^{2+} gradually converts the original single sigmoid aggregation kinetics to a biphasic process under the current experimental condition. In particular, two distinct aggregation phases were clearly identified in the presence of 10 μM or higher concentration of Zn^{2+} (Fig. 1A). Here, we define the t_{50} of the second phase as the time at which the fluorescence intensity reaches the midpoint of the first stationary phase and the maximum of the ThT fluorescence intensity measured at the end of the experiment. Under the current experimental condition, Zn^{2+} delays the appearance of the second aggregation phase remarkably in a dose-dependent manner (Fig. 1D). For instance, in the presence of 10 μM Zn^{2+}, the t_{50} of the second aggregation phase is ~35 h, ~3-folds of that of the single sigmoid kinetics of Aβ40 only. Higher amount of Zn^{2+} leads to a larger t_{50} value of the second aggregation phase. The final intensity of the fluorescence of the second phase also decreases with increased concentration of Zn^{2+} (Fig. 1E). These results suggest that Zn^{2+}, although initiating and facilitating a fast aggregation process, can significantly delay the second aggregation phase during Aβ amyloid formation. This is probably in accord with some previous studies suggesting the inhibitory activity of Zn^{2+} on Aβ40 amyloidogenesis [10]. The morphology of the amyloids formed in the first stationary phase (time point III in Fig. 1A), as depicted in Fig. 1K, is similar to that observed in the first growth phase (Fig. 1J) and the amyloid imaging acquired after 3 d incubation (Fig. 1L), while the amyloid fibrils of Aβ40 only collected at the end of the kinetics experiment (Fig. 1H) are curlier in comparison to that of Aβ40 with Zn^{2+}.

Zn^{2+} has been reported to coordinate with Aβ via interacting with the N-terminal hydrophilic region of the peptide, especially the three histidine residues, His6, His13 and His14 [7]. These interactions could putatively arrange the N-terminal region into a more ordered conformation to some extent, and further favor the intermolecular hydrophobic interactions to initiate nucleation, thus promoting the formation of oligomeric nuclei for the onset of a fast early aggregation phase. At the acidic pH of 5.0, there is no significant change of the aggregation kinetics of Aβ40 when Zn^{2+} is added (Fig. S1). This suggests the importance of His residues involved in the interactions with the metal ion. At this pH value, the His residues are largely protonated and contain positive charge which may impair the coordination of Zn^{2+} with the peptide, thus reducing the kinetic influence of Zn^{2+} on Aβ aggregation.

The Zn^{2+}-induced dose-dependent retardation of the second

aggregation phase could be due to a number of possible reasons. It may be attributed to the aggregation of the remaining free Aβ monomers that do not coordinate with Zn^{2+} and are not involved in the fast aggregation process. Increasing the concentration of Zn^{2+} can facilitate the self-assembly of Aβ during the first aggregation phase and therefore decrease the amount of free Aβ remained in solution, which may lead to a retarded secondary aggregation. Alternatively, the second aggregation phase may be correlated to a morphological rearrangement of the aggregates formed in the first phase to form the aggregated structures that bind more efficiently with ThT. In either plausible scenario, the results suggest that the amyloids formed in the presence of Zn^{2+} might have different packing properties between the monomeric molecules compared to those formed without Zn^{2+}, although the morphology of the amyloid fibrils formed in both conditions is comparable as shown in the AFM imaging results. The CD spectrum of the fresh Aβ40 (Fig. 2) suggests a random coil structure of the peptide in solution. Over the incubation period, a negative band at ~216 nm appears with a positive band at ~195 nm, suggesting the formation of β-sheet-like structures upon aggregation. In the presence of Zn^{2+}, the band change in the CD spectra over time becomes slower and more complex (Fig. 2). It was suggested that the orientation and twisting of β-sheets can affect the CD characteristics of proteins and amyloids [25]. Our results imply that the amyloid fibrils of Aβ40 co-incubating with Zn^{2+} may contain different structural characteristics such as distinct twisting angles of the β-strand in the aggregates. This also indicates that Zn^{2+} can modulate Aβ aggregation at different stages including both the early oligomerization and the subsequent elongation phase, and the overall impact is concentration sensitive.

Although it has been well recognized that Aβ generally undergoes a typical sigmoidal kinetics during aggregation, the emergence of biphasic aggregation kinetics of Aβ has recently been reported by different research groups [26–29]. For instance, by studying a dimAβ, in which two Aβ40 unites were connected through a flexible glycine-serine-rich linker, Hasecke et al. found that increasing peptide concentration above a critical value converted the aggregation kinetics from sigmoidal to biphasic [28], including a lag-free initial phase linked to the formation of off-pathway oligomers and a second phase attributed to fibril nucleation and growth. Their results also suggested that the off-pathway oligomers compete with fibrils for monomers and inhibit the autocatalytic amplification of amyloid fibrils, leading to the retardation of the second aggregation phase [29]. These studies highlight the sensitivity of the mechanistic details of protein aggregation on the specific experimental conditions and environments. Factors such as protein concentration and metal ions may significantly modify the aggregation pathway of proteins. Here in this study, Zn^{2+} promotes the formation of oligomeric nuclei and fibrillar structures in the first aggregation phase. This probably indicates that the oligomers formed in the presence of Zn^{2+} are efficient on-pathway nuclei favorable for further growth to form fibrils.

3.2. Effect of carnosine on Aβ40 aggregation kinetics

Carnosine is a bioactive molecule that has been indicated to provide protective benefits for counteracting to neurodegenerative conditions [30]. Recent studies reported that carnosine can inhibit the aggregation of amyloidogenic proteins such as α-crystallin and Aβ42 [21,31,32], which may ameliorate the toxicity of protein aggregates. The aggregation kinetics results here show that the presence of a high concentration of carnosine decreases the ThT fluorescence intensity in the final plateau phase of Aβ40 aggregation (Fig. 3). For instance, the final ThT fluorescence intensity drops ~20% in the presence of 5 mM carnosine (Fig. 3B). There is a ~53% drop in the ThT fluorescence intensity when 10 mM carnosine is added. These results are in accord with the previous reports of the inhibitory activity of carnosine on the aggregation of Aβ42 [21, 32]. The addition of low concentration of carnosine, e.g., 1 mM or lower, does not decrease the final ThT fluorescence intensity dramatically, indicating a relatively modest inhibitory activity of the compound on Aβ40 aggregation. In addition, the addition of carnosine exerts little effect on the lag time of the aggregation kinetics, and the t_{50} values of the aggregation kinetics without or in the presence of different amount of carnosine are similar (Fig. 3C). A previous study by Attanasio et al. suggested that carnosine can bind to Aβ42 peptide and perturb the hydrogen bonding network in and around the central hydrophobic cluster, which may block the fibrillogenesis pathway of Aβ42 [21]. The weak influence of carnosine on the lag phase and t_{50} of Aβ40 aggregation observed here suggests that the interaction of carnosine and Aβ40 does not significantly perturb the early oligomerization process toward forming the crucial aggregation nucleus. Instead, it might interfere to some extent with the growth of oligomeric nuclei to form amyloid fibrils. The relatively high concentration of carnosine required for suppressing amyloid formation indicates a weak interaction of carnosine and the peptide.

3.3. Effect of carnosine on Zn^{2+}-mediated Aβ40 aggregation

One of the characteristic functions of carnosine is its capability to chelate with metal ions including Zn^{2+} [33]. It has been reported that carnosine coordinates to Zn^{2+} as a quadridentate ligand [34]. It is indicated that carnosine may contribute to the regulation of Zn^{2+} availability in the brain [35]. Therefore, in addition to directly interacting with Aβ to modulate its aggregation properties, carnosine may also influence Aβ aggregation in vivo indirectly by interacting with metal ions such as Zn^{2+}. To assess the impact of carnosine on Zn^{2+}-mediated Aβ aggregation, we measured the aggregation kinetics of Aβ40 (10 μM) in the presence of Zn^{2+} (10 μM) and different amounts of carnosine. As shown in Fig. 4, the addition of carnosine with a

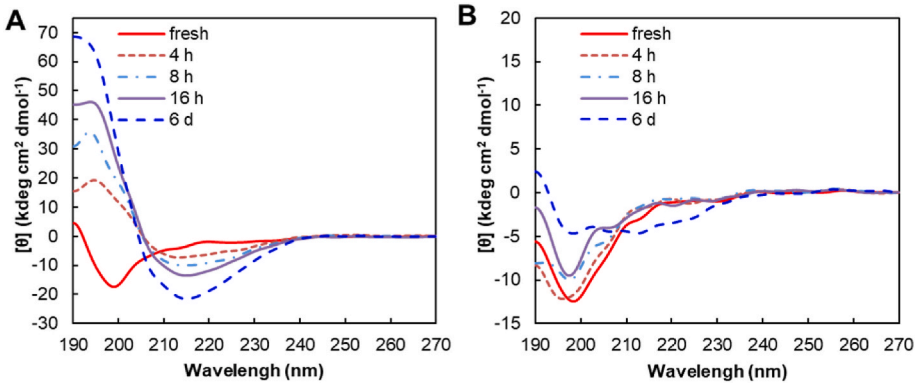

Fig. 2. CD spectra of Aβ40 (50 μM) alone (A) and in the presence of 50 μM Zn^{2+} (B). The peptide was incubated quiescently at 37 °C in pH 7.4 phosphate buffer (10 mM Na-phosphate) and the spectra were measured at various time points of the incubation period.

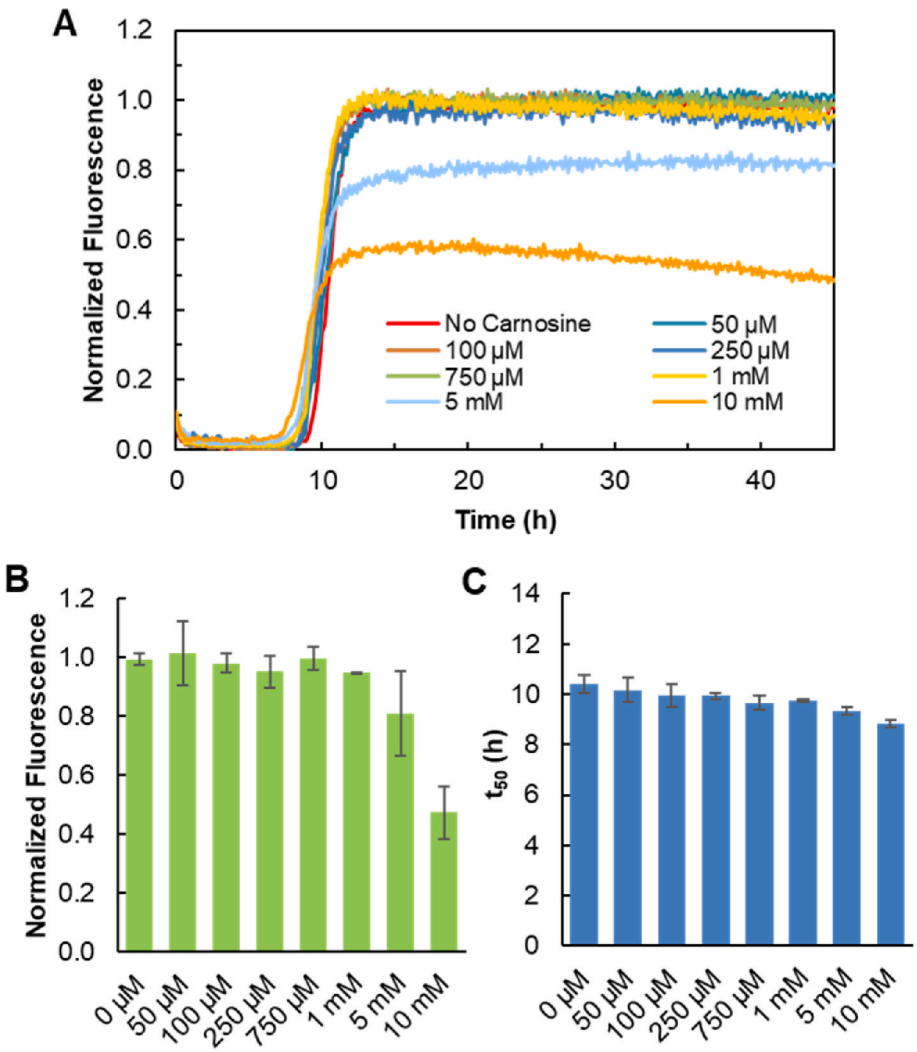

Fig. 3. Effect of carnosine on Aβ40 aggregation. (A) Aggregation kinetics of Aβ40 (10 μM) alone and in the presence of different concentrations of carnosine followed by ThT fluorescence at 37 °C in pH 7.4 phosphate buffer (50 mM Na-phosphate). (B) Relative ThT fluorescence intensity at the end of the aggregation kinetics of Aβ40 in the absence or presence of different concentrations of carnosine. The data are reported as mean ± standard deviation of triplicate results. (C) The half time (t_{50}) of the aggregation kinetics of Aβ40 shown in panel A.

concentration up to 2.5 mM gradually accelerates the aggregation rate in the second aggregation phase. The t_{50} value of the second aggregate phase decreases in a manner that correlates with the carnosine concentration (Fig. 4C). This is most likely because that carnosine chelates with Zn^{2+} and therefore impairs the activity of Zn^{2+} on retarding the second aggregation kinetics.

In the meantime, the addition of carnosine also suppresses the early aggregation phase induced by Zn^{2+} (Fig. 4B). The ThT fluorescence intensity in this early phase diminishes with the increase of carnosine. In the presence of 5 mM carnosine, the early aggregation phase is significantly suppressed and barely detectable (Fig. 4B). The aggregation kinetics is essentially converted back to a single sigmoidal trace, while the half time of the aggregation kinetics is still longer than that of Aβ without Zn^{2+}. The addition of 10 mM carnosine largely eliminates the influence of Zn^{2+} on Aβ aggregation, and the kinetics trace becomes comparable to that of Aβ only. This is most likely due to the chelation of most of Zn^{2+} by carnosine, thus eliminating the impact of Zn^{2+} on aggregation. Our results also suggest that Zn^{2+}-carnosine complex probably does not bind to Aβ efficiently, showing little impact on peptide aggregation. The effect of carnosine on Zn^{2+}-mediated Aβ aggregation was also confirmed by AFM (Fig. S2). The presence of 10 mM carnosine strongly suppressed Zn^{2+}-induced fast formation of fibrillar structures, whereas low amount of carnosine (100 μM) did not effectively inhibit Aβ40 fibril formation during the first aggregation phase, consistent with the ThT kinetics results.

In this study, we have investigated the kinetic impact of Zn^{2+} on the aggregation of Aβ40 peptide. Our results show a transition of the aggregation kinetics from a single sigmoidal to a biphasic process upon the presence of Zn^{2+}. As illustrated in Fig. 5, the interactions of Zn^{2+} and the peptide can facilitate the self-assembly of monomers to form on-pathway oligomeric intermediates, which further grow to form fibrils in the first fast aggregation phase. The second aggregation phase of Aβ40 is retarded by Zn^{2+} in a dose-dependent manner. The future cytotoxicity studies on oligomers and amyloids formed during the first and second aggregation stages will provide insight into the influence of this metal ion on Aβ toxicity. Elucidation of the structural characteristics of Aβ aggregates formed at different stages of the aggregation using high resolution methods such as NMR will also be crucial for understanding the mechanistic role of Zn^{2+} in regulating Aβ cytotoxicity. In addition, our results show that carnosine has weak effect on the aggregation kinetics of Aβ40, although high concentration of carnosine mildly inhibits Aβ40 aggregation which is consistent with previous studies [21]. Furthermore, our study shows that carnosine remarkably decreases the activity of Zn^{2+} on modulating Aβ aggregation, most likely via the coordination with the metal ion to form chelate (Fig. 5). The results indicate a promising in vivo protective effect of this natural dipeptide against Aβ cytotoxicity by suppressing Zn^{2+}-induced rapid oligomerization and fibrillation of Aβ under physiological conditions.

Declaration of cometing interest

The authors declare that they have no known competing financial

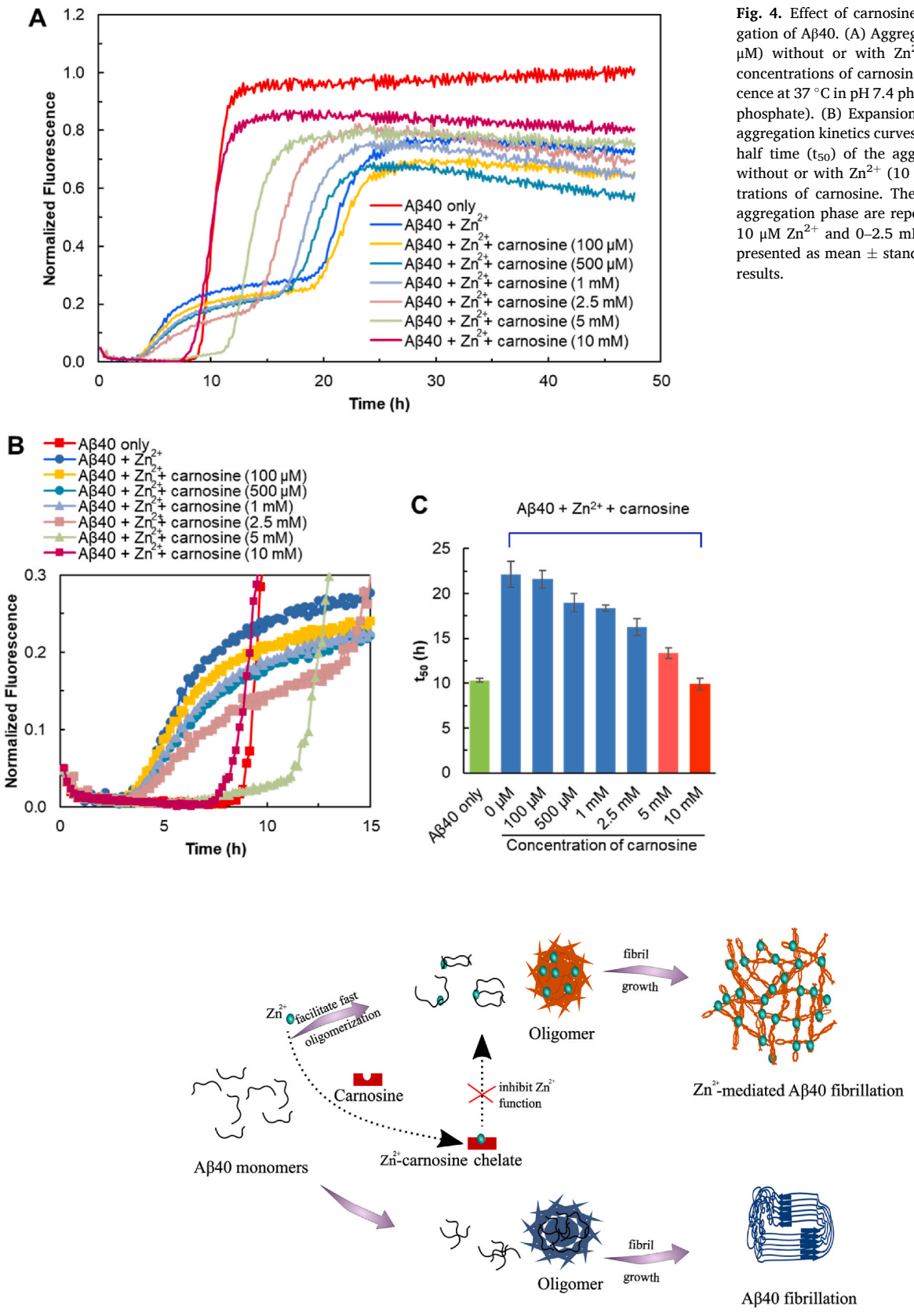

Fig. 4. Effect of carnosine on Zn^{2+}-mediated aggregation of Aβ40. (A) Aggregation kinetics of Aβ40 (10 μM) without or with Zn^{2+} (10 μM) and different concentrations of carnosine followed by ThT fluorescence at 37 °C in pH 7.4 phosphate buffer (50 mM Na-phosphate). (B) Expansion of the early stage of the aggregation kinetics curves shown in panel A. (C) The half time (t_{50}) of the aggregation kinetics of Aβ40 without or with Zn^{2+} (10 μM) and different concentrations of carnosine. The t_{50} values of the second aggregation phase are reported for the samples with 10 μM Zn^{2+} and 0–2.5 mM carnosine. The data are presented as mean ± standard deviation of triplicate results.

Fig. 5. Schematic diagram of the proposed effects of Zn^{2+} and carnosine on the aggregation pathway of Aβ40.

interests or personal relationships that could have appeared to influence the work reported in this paper.

Acknowledgements

D.D. gratefully acknowledges the financial support from the National Institutes of Health (R15GM116006) and the Alzheimer's Association (AARG-17-531423).

Appendix A. Supplementary data

Supplementary data to this article can be found online at https://doi.org/10.1016/j.bbrep.2022.101333.

References

[1] R.E. Tanzi, L. Bertram, Twenty years of the Alzheimer's disease amyloid hypothesis: a genetic perspective, Cell 120 (2005) 545–555.
[2] A. M Grabrucker, M. Rowan, C. C Garner, Brain-delivery of zinc-ions as potential treatment for neurological diseases: mini review, Drug Deliv. Lett. 1 (2011) 13–23.
[3] W.R. Markesbery, W.D. Ehmann, M. Alauddin, T. Hossain, Brain trace element concentrations in aging, Neurobiol. Aging 5 (1984) 19–28.
[4] A. Takeda, S. Takefuta, S. Okada, N. Oku, Relationship between brain zinc and transient learning impairment of adult rats fed zinc-deficient diet, Brain Res. 859 (2000) 352–357.
[5] L.M. Miller, Q. Wang, T.P. Telivala, R.J. Smith, A. Lanzirotti, J. Miklossy, Synchrotron-based infrared and X-ray imaging shows focalized accumulation of Cu and Zn co-localized with β-amyloid deposits in Alzheimer's disease, J. Struct. Biol. 155 (2006) 30–37.
[6] M. Lovell, J. Robertson, W. Teesdale, J. Campbell, W. Markesbery, Copper, iron and zinc in Alzheimer's disease senile plaques, J. Neurol. Sci. 158 (1998) 47–52.
[7] V. Minicozzi, F. Stellato, M. Comai, M. Dalla Serra, C. Potrich, W. Meyer-Klaucke, S. Morante, Identifying the minimal copper-and zinc-binding site sequence in amyloid-β peptides, J. Biol. Chem. 283 (2008) 10784–10792.
[8] N.G. Nair, G. Perry, M.A. Smith, V.P. Reddy, NMR studies of zinc, copper, and iron binding to histidine, the principal metal ion complexing site of amyloid-β peptide, J. Alzheim. Dis. 20 (2010) 57–66.
[9] Y. Yoshiike, K. Tanemura, O. Murayama, T. Akagi, M. Murayama, S. Sato, X. Sun, N. Tanaka, A. Takashima, New insights on how metals disrupt amyloid β-aggregation and their effects on amyloid-β cytotoxicity, J. Biol. Chem. 276 (2001) 32293–32299.
[10] A. Abelein, A. Gräslund, J. Danielsson, Zinc as chaperone-mimicking agent for retardation of amyloid β peptide fibril formation, Proc. Natl. Acad. Sci. U.S.A. 112 (2015) 5407–5412.
[11] A.I. Bush, W.H. Pettingell, G. Multhaup, M.d. Paradis, J.-P. Vonsattel, J.F. Gusella, K. Beyreuther, C.L. Masters, R.E. Tanzi, Rapid induction of Alzheimer Aβ amyloid formation by zinc, Science 265 (1994) 1464–1467.
[12] J. Guo, L. Yu, Y. Sun, X. Dong, Kinetic insights into Zn2+-induced amyloid β-protein aggregation revealed by stopped-flow fluorescence spectroscopy, J. Phys. Chem. B 121 (2017) 3909–3917.
[13] M.-C. Lee, W.-C. Yu, Y.-H. Shih, C.-Y. Chen, Z.-H. Guo, S.-J. Huang, J.C. Chan, Y.-R. Chen, Zinc ion rapidly induces toxic, off-pathway amyloid-β oligomers distinct from amyloid-β derived diffusible ligands in Alzheimer's disease, Sci. Rep. 8 (2018) 1–16.
[14] V. Tõugu, A. Karafin, K. Zovo, R.S. Chung, C. Howells, A.K. West, P. Palumaa, Zn (II)-and Cu (II)-induced non-fibrillar aggregates of amyloid-β (1-42) peptide are transformed to amyloid fibrils, both spontaneously and under the influence of metal chelators, J. Neurochem. 110 (2009) 1784–1795.
[15] Y. Miller, B. Ma, R. Nussinov, Zinc ions promote Alzheimer Aβ aggregation via population shift of polymorphic states, Proc. Natl. Acad. Sci. U.S.A. 107 (2010) 9490–9495.
[16] A.A. Boldyrev, G. Aldini, W. Derave, Physiology and pathophysiology of carnosine, Physiol. Rev. 93 (2013) 1803–1845.
[17] S.E. Gariballa, A.J. Sinclair, Carnosine: physiological properties and therapeutic potential, Age Ageing 29 (2000) 207–210.
[18] V.P. Reddy, M.R. Garrett, G. Perry, M.A. Smith, Carnosine: a versatile antioxidant and antiglycating agent, Sci. Aging Knowl. Environ. 18 (2005) pe12-pe12.
[19] C. Corona, V. Frazzini, E. Silvestri, R. Lattanzio, R. La Sorda, M. Piantelli, L. M. Canzoniero, D. Ciavardelli, E. Rizzarelli, S.L. Sensi, Effects of dietary supplementation of carnosine on mitochondrial dysfunction, amyloid pathology, and cognitive deficits in 3xTg-AD mice, PLoS One 6 (2011), e17971.
[20] M. Kawahara, H. Koyama, T. Nagata, Y. Sadakane, Zinc, copper, and carnosine attenuate neurotoxicity of prion fragment PrP106-126, Metallomics 3 (2011) 726–734.
[21] F. Attanasio, M. Convertino, A. Magno, A. Caflisch, A. Corazza, H. Haridas, G. Esposito, S. Cataldo, B. Pignataro, D. Milardi, Carnosine inhibits Aβ42 aggregation by perturbing the H-bond network in and around the central hydrophobic cluster, Chembiochem 14 (2013) 583–592.
[22] G. Caruso, C.G. Fresta, N. Musso, M. Giambirtone, M. Grasso, S.F. Spampinato, S. Merlo, F. Drago, G. Lazzarino, M.A. Sortino, Carnosine prevents Aβ-induced oxidative stress and inflammation in microglial cells: a key role of TGF-β1, Cells 8 (2019) 64.
[23] C. Morris, S. Cupples, T.W. Kent, E.A. Elbassal, E.P. Wojcikiewicz, P. Yi, D. Du, N-Terminal charged residues of amyloid-beta peptide modulate amyloidogenesis and interaction with lipid membrane, Chem. Eur J. 24 (2018) 9494–9498.
[24] H. Liu, R. Lantz, P. Cosme, N. Rivera, C. Andino, W.G. Gonzalez, A.C. Terentis, E. P. Wojcikiewicz, R. Oyola, J. Miksovska, Site-specific dynamics of amyloid formation and fibrillar configuration of Aβ 1–23 using an unnatural amino acid, Chem. Commun. 51 (2015) 7000–7003.
[25] A. Micsonai, F. Wien, L. Kernya, Y.-H. Lee, Y. Goto, M. Réfrégiers, J. Kardos, Accurate secondary structure prediction and fold recognition for circular dichroism spectroscopy, Proc. Natl. Acad. Sci. U.S.A. 112 (2015) E3095–E3103.
[26] M. Nick, Y. Wu, N.W. Schmidt, S.B. Prusiner, J. Stöhr, W.F. DeGrado, A long-lived Aβ oligomer resistant to fibrillization, Biopolymers 109 (2018), e23096.
[27] Z. Fu, D. Aucoin, J. Davis, W.E. Van Nostrand, S.O. Smith, Mechanism of nucleated conformational conversion of Aβ42, Biochemistry 54 (2015) 4197–4207.
[28] F. Hasecke, T. Miti, C. Perez, J. Barton, D. Schölzel, L. Gremer, C.S. Grüning, G. Matthews, G. Meisl, T.P. Knowles, Origin of metastable oligomers and their effects on amyloid fibril self-assembly, Chem. Sci. 9 (2018) 5937–5948.
[29] F. Hasecke, C. Niyangoda, G. Borjas, J. Pan, G. Matthews, M. Muschol, W. Hoyer, Protofibril–fibril interactions inhibit amyloid fibril assembly by obstructing secondary nucleation, Angew. Chem. Int. Ed. 60 (2021) 3016–3021.
[30] S. Banerjee, B. Mukherjee, M.K. Poddar, G.L. Dunbar, Carnosine improves aging-induced cognitive impairment and brain regional neurodegeneration in relation to the neuropathological alterations in the secondary structure of amyloid beta (Aβ), J. Neurochem. 158 (2021) 710–723.
[31] F. Attanasio, S. Cataldo, S. Fisichella, S. Nicoletti, V.G. Nicoletti, B. Pignataro, A. Savarino, E. Rizzarelli, Protective effects of L-and D-carnosine on α-crystallin amyloid fibril formation: implications for cataract disease, Biochemistry 48 (2009) 6522–6531.
[32] A. Aloisi, A. Barca, A. Romano, S. Guerrieri, C. Storelli, R. Rinaldi, T. Verri, Anti-aggregating effect of the naturally occurring dipeptide carnosine on Aβ1-42 fibril formation, PLoS One 8 (2013), e68159.
[33] C.E. Brown, W.E. Antholine, Chelation chemistry of carnosine. Evidence that mixed complexes may occur in vivo, J. Phys. Chem. 83 (1979) 3314–3319.
[34] T. Matsukura, T. Takahashi, Y. Nishimura, T. Ohtani, M. Sawada, K. Shibata, Characterization of crystalline L-carnosine Zn (II) complex (Z-103), a novel anti-gastric ulcer agent: tautomeric change of imidazole moiety upon complexation, Chem. Pharm. Bull. 38 (1990) 3140–3146.
[35] M.C. Udechukwu, S.A. Collins, C.C. Udenigwe, Prospects of enhancing dietary zinc bioavailability with food-derived zinc-chelating peptides, Food Funct. 7 (2016) 4137–4144.